Comput Visual Sci 5: 45–51 (2002)
Digital Object Identifier (DOI) 10.1007/s00791-002-0086-4

Computing and
Visualization in Science

Regular article

Visualising deformation fields computed by non-linear image registration

Marc Tittgemeyer, Gert Wollny, Frithjof Kruggel

Max-Planck-Institute of Cognitive Neuroscience, Stephanstr. 1a, 04103 Leipzig, Germany
(e-mail: {tittge, wollny, kruggel}@cns.mpg.de)

Received: 27 September 2001 / Accepted: 19 March 2002

Communicated by: C. Johnson and M. Rumpf

Abstract. Magnetic resonance imaging (MRI) is used in clinical routine to map the brain's morphology. Structural changes due to brain growth, ageing, surgical intervention or pathological processes may be detected by non-linear image registration of time-series imaging data. The resulting displacement field is large and therefore, hard to interpret. For a simplified but sufficient description of the displacement field contraction mapping is proposed to detect vector field singularities. This allows the detection and analysis of singularities of any order as critical points which reflect the topology of the vector field. An application demonstrates how this method helps to increase the understanding of pathological processes in the brain.

1 Introduction

High-dimensional vector fields are a result of observed measurements or simulated processes in a variety of application domains (e.g., geophysics, meteorology, or medicine). In order to improve the understanding of underlying dynamics it is useful to characterize the vector field by its critical points. The most prominent critical points are attractors, repellors and vortices (rotation centers). A concise classification scheme for critical points (Fig. 1) by their so-called phase portrait has been introduced by Abraham and Shaw [1]. Critical points characterize a high-dimensional vector field as a sparse set of features that are sufficient to understand the behaviour of the simulated physical process and its topology.

However, the detection and visualization of critical points is still an active research area where rather sophisticated mathematical methods have been employed [12]. Established are topological methods as introduced by Helman and Hesselink [13] that decompose vector fields in different global regions of interest based on local linear approximations of the Jacobian. Higher-order approximations yield different decompositions [22]. Philippou and Strickland [19] introduced a geometrical method where critical points are found at the intersection of lines tangent with the vector orientation (or at the intersection of planes orthogonal to the vectors). Other widely employed methods are based on the Poincaré-Hopf index theorem (e.g., [10]).

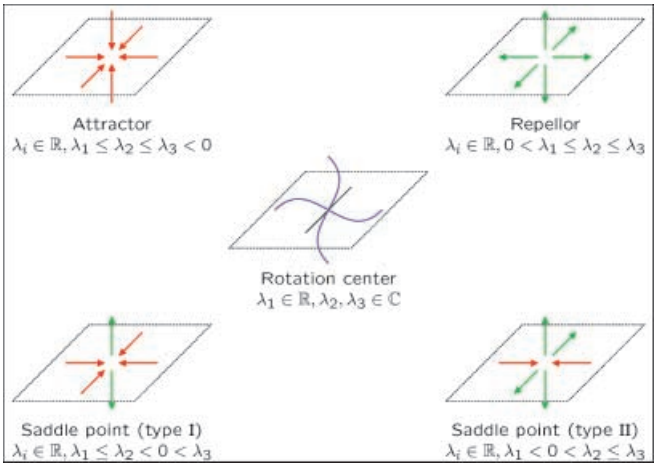

Fig. 1. Classification criteria for critical points (after Abraham and Shaw [1]). λ_i denote the eigenvalues of the phase portrait to a critical point

In our application, changes of brain structure due to brain growth, ageing, surgical intervention or pathological processes are monitored by time-series examinations using magnetic resonance imaging (MRI). MR images are given as 3D matrices of intensity values. Beyond usual comparison of the image data, which is still the gold standard in clinical neuroscience, structural changes with time may be detected by non-linear registration of the imaged brain. The result of the registration algorithm is a vector field which maps one image onto another. This displacement field reflects the structural change that acted on the brain.

Due to the finite spatial resolution of the images, the displacement field is given on a discrete grid. Since, for example, growth or atrophying processes take place in finite sub-compartments of the brain, representing critical points

by point sources is an over-simplification. Most conventional methods fail therefore to detect critical points within medical vector fields. Thus, in our application critical points are not regarded as infinitesimally small.

We rather propose a novel method that is based on contraction mapping. For an application to a patient suffering from neurodegeneration we will illustrate how non-rigid registration and critical points analysis may help to understand the disease process.

2 Non-rigid image registration

Image registration is usually achieved by applying a vector field transformation to one image (study) in order to match another (reference) image. Typically, an image is given as mapping $I : \Omega \to V$ from the image coordinate-domain $\Omega \subseteq \mathbb{R}^n$ to its intensity range $V \subseteq \mathbb{R}$. The ordered pair $(\boldsymbol{x}, I(\boldsymbol{x}))$ is called a voxel (volume element) of the image, with $\boldsymbol{x} \in \Omega$ being an image coordinate. We refer to the study image as $S : \Omega \to V$ and the reference as $R : \Omega \to V$. Ideally, the registration aims to determine a transformation $\boldsymbol{T} : \Omega \to \Omega$ such that $S(\boldsymbol{T}(\boldsymbol{x})) = R(\boldsymbol{x})$. The set of all transformations that change an image according to $I_T := I(\boldsymbol{T}(\boldsymbol{x}))$ is called the transformation space Γ.

In our application, transformations correspond to spatial displacements $\boldsymbol{u}$ of voxels and are described in the so-called *Eulerian* reference frame. The set of the displacements of all voxels of an image is called a displacement field over domain Ω, its value at time t is denoted as $\boldsymbol{u}(t)$. The corresponding transformation $\boldsymbol{T}$ can be given coordinate-wise:

$$\boldsymbol{T}(\boldsymbol{x}, t) := \boldsymbol{x} - \boldsymbol{u}(\boldsymbol{x}, t) \quad \forall \boldsymbol{x} \in \Omega \,. \tag{1}$$

The focus of registration is now to find a transformation $T_{\min} \in \Gamma$ that minimizes a given cost function $F(R, S_T)$ in conjunction with an energie regularisation. This function describes the similarity between the transformed study image S_T and reference image R and is usually further constraint with an energy normalization (smoothness) term $E(T)$ that enforces topology preservation:

$$T_{\min} := \arg\min_{T \in \Gamma} \left(F(R, S_T) + \kappa E(T) \right) \,. \tag{2}$$

Here, κ is a Lagrangian multiplier to balance between registration accuracy and transformation smoothness. A common approach to solve the minimization problem (2) is to find the root of its first order derivative

$$\kappa \frac{\partial}{\partial T} E(T) = -\frac{\partial}{\partial T} F(R, S_T) \,. \tag{3}$$

A rigid registration restricts the transformation space Γ to translation and rotation only. If the transformation is not restricted a priori, then the registration is called *non-rigid* or *deformable*.

In our application, global image variability such as position and orientation differences of subjects head have to be removed prior to further image processing. This is carried out by a rigid registration scheme [23]. To obtain knowlegde about the morphological (local) change, non-rigid registration has to be employed subsequently. The mathematical framework to carry out such task with respect to the discipline of computational anatomy has been compiled by Grenander and Miller [11].

Image matching of deformable structures has received considerable attention during the last decade [16]. The high dimensional transformations involved in deformable registration generally make the problem ill-conditioned (i.e., many possible solutions exists), so that additional constraints are needed [2, 3, 9, 17]. Recently, Musse et al. [18] or Christensen and Johnson [7] address also the topological issues involved with small- and large-distance, non-linear transformations.

Bio-mechanically plausible transformations are constrained to be consistent with the physical properties of deformable elastic solids. To understand how elastic image matching works, consider the deforming image to be embedded in a 3D elastic medium. The medium is subjected to distributed internal forces, which reconfigure it, and lead the image to match a target. In linear elastic media, the displacement vector field $\boldsymbol{u}(\boldsymbol{x})$ resulting form internal driving forces $\boldsymbol{f}(\boldsymbol{x})$ (called *body forces*) obeys the Navier-Stokes equilibrium equations for linear elasticity:

$$\mu \nabla^2 \boldsymbol{u} + (\lambda + \mu) \boldsymbol{\nabla} (\boldsymbol{\nabla} \cdot \boldsymbol{u}) = -\boldsymbol{f}(\boldsymbol{u}) \,, \quad \forall \boldsymbol{x} \in \Omega \,. \tag{4}$$

Here, $\boldsymbol{\nabla} \cdot \boldsymbol{u} = \sum \partial u_j / \partial x_j$ is the cubical dilatation of the medium, ∇^2 is the Lagrangian operator, and Lamé's coefficients λ and μ refer to the elastic properties of the medium; λ controls the rate of growth or shrinkage of a local region whereas μ controls the shearing between adjacent regions of the image. With $T(\boldsymbol{x}) := \boldsymbol{x} - \boldsymbol{u}(\boldsymbol{x})$, $\frac{\partial}{\partial T} F(R, S_T) := \boldsymbol{f}(\boldsymbol{u})$, $\kappa := 1.0$, and $\frac{\partial}{\partial T} E(T) := \mu \nabla^2 \boldsymbol{u} + (\lambda + \mu) \boldsymbol{\nabla} (\boldsymbol{\nabla} \cdot \boldsymbol{u})$, (4) corresponds to the registration minimization problem (3).

However, the assumption of linear elasticity restricts the registration to be globally smooth and therefore to accommodate only small deformations. In an extension to his initial work [5], Christensen [6] described a registration approach in which a viscous fluid model was used to control the deformation.

For viscous fluids, the force $\boldsymbol{f}(\boldsymbol{u})$ is proportional to the time rate of change in displacement. The PDE describing the fluid transformation of the study image is given by (see Christensen et al. [8] for a detailed derivation)

$$\nabla^2 \boldsymbol{v} + (\lambda + \mu) \boldsymbol{\nabla} (\boldsymbol{\nabla} \cdot \boldsymbol{v}) = -\boldsymbol{f}(\boldsymbol{u}) \,, \tag{5}$$

where $\boldsymbol{v}$ is the instantaneous velocity of the displacement field $\boldsymbol{u}$. The $\nabla^2 \boldsymbol{v}$ term in (5) is the viscous term of the PDE. This term constrains the velocity of the neighbouring particles of the displacement field to vary smoothly.

Due to attenuation in viscous fluids, internal forces disappear with time in this model. Thus, the desired deformation can be fully achieved, even if large deformations are required. By applying the *sum of squared differences*

$$F_{\mathrm{SSD}}(T, S, R) := \int_{\Omega} \left(S(T(\boldsymbol{x})) - R(\boldsymbol{x}) \right)^2 d\boldsymbol{x} \tag{6}$$

as a cost function, (5) can be rewritten as

$$\begin{aligned} &\mu \nabla^2 \boldsymbol{v}(\boldsymbol{x}, t) + (\mu + \lambda) \nabla (\nabla \cdot) \boldsymbol{v}(\boldsymbol{x}, t) \\ &\quad = -\left[S\left(\boldsymbol{x} - \boldsymbol{u}(\boldsymbol{x}, t)\right) - R(\boldsymbol{x}) \right] \nabla S|_{\boldsymbol{x} - \boldsymbol{u}(\boldsymbol{x}, t)} \,. \end{aligned} \tag{7}$$

In order to solve the registration problem, the continous domain Ω is discretized, and (7) is approximated using a finite difference scheme [21].

Then, registration is achieved iteratively over a time step of Δt. In each step, (5) is solved for constant time to estimate the current velocity field $\boldsymbol{v}$ which is then used to update the displacement field $\boldsymbol{u}$ by a time integration step [6]

$$\boldsymbol{u}(\boldsymbol{x}, t+\Delta t) := \boldsymbol{u}(\boldsymbol{x}, t) + \Delta t\,[\boldsymbol{v}(\boldsymbol{x}, t) - \nabla \boldsymbol{u}(\boldsymbol{x}, t)\boldsymbol{v}(\boldsymbol{x}, t)]\ . \quad (8)$$

To avoid local minima of the minimization problem (2), and to speed up the computation, a coarse-to-fine multi-resolution approach is employed [24], i.e. the domain Ω is first discretized using a coarse grid. After solving the registration problem on the coarse grid, the discretization is refined. The registration transformation is propagated to this refined grid, and used as starting point when searching the refined solution. As in our application the images have a finite resolution, i.e. they are usually not defined on the continous domain Ω but on a on a finite grid, their resolution can be seen as a natural breaking condition for the multi-resolution step.

Wollny and Kruggel [26] proposed a fast algorithm to carry out non-rigid registration based on fluid dynamical modelling [25].

3 The Concept of Critical Points

Consider a vector field $\boldsymbol{u} : \Omega \to \mathbb{R}^3$ for some compact domain $\Omega \subseteq \mathbb{R}^3$ and the set:

$$U_\varepsilon\left(\boldsymbol{x}'\right) := \left\{\boldsymbol{x} |\ \| \boldsymbol{x} - \boldsymbol{x}' \| < \varepsilon, \boldsymbol{x} \in \Omega\right\}\ , \quad (9)$$

for any $\varepsilon > 0, \varepsilon \in \mathbb{R}$ and a $\boldsymbol{x}' \in \Omega$; the set U_ε is called the *ε-environment* of $\boldsymbol{x}'$.

The Taylor series expansion of $\boldsymbol{u}(\boldsymbol{x})$ around the point $\boldsymbol{x}'$ yields:

$$\boldsymbol{u}(\boldsymbol{x}) = \left.\frac{\partial u_i}{\partial x_j}\right|_{\boldsymbol{x}'} \left(\boldsymbol{x} - \boldsymbol{x}'\right) + \boldsymbol{u}\left(\boldsymbol{x}'\right) + O(\boldsymbol{x})\,.$$

By taking into account only its linear terms, and with the substitution $\boldsymbol{A} := \left.\frac{\partial u_i}{\partial x_j}\right|_{\boldsymbol{x}'}$, $\boldsymbol{A} \in \mathbb{R}^{3\times 3}$ we obtain

$$\boldsymbol{u}(\boldsymbol{x}) = \boldsymbol{A}\left(\boldsymbol{x} - \boldsymbol{x}'\right) + \boldsymbol{u}\left(\boldsymbol{x}'\right)\ . \quad (10)$$

Thus, we can now define (cf. [19]):

Definition 1. *A critical point $\boldsymbol{x}_{cp}$ is an equilibrium point in the vector field topology where $\boldsymbol{u}(\boldsymbol{x}_{cp}) = 0$ while there exists an $\varepsilon > 0, \varepsilon \in \mathbb{R}$ so that $\boldsymbol{u}(\boldsymbol{x}) \neq 0\, \forall\, \boldsymbol{x} \in U_\epsilon(\boldsymbol{x}_{cp}) \backslash \{\boldsymbol{x}_{cp}\}$.*

Proposition 1. *Within the vicinity of a critical point $\boldsymbol{x}_{cp}$, the vector field $\boldsymbol{u}(\boldsymbol{x})$ – as it is outlined in* (10) *– can be approximated by*

$$\boldsymbol{u}(\boldsymbol{x}) = \boldsymbol{A}\left(\boldsymbol{x} - \boldsymbol{x}_{cp}\right)\ ,$$

where the matrix $\boldsymbol{A}$ is called the phase portrait of the critical point $\boldsymbol{x}_{cp}$.

As a first-order Taylor series would have a limited scope in modelling $\boldsymbol{u}(\boldsymbol{x})$ adequately, i.e., the influence of critical point $\boldsymbol{x}_{\mathrm{cp}}$ would decay with distance $\Delta\boldsymbol{x} = \boldsymbol{x} - \boldsymbol{x}_{\mathrm{cp}}$, accuracy in modelling can be increased by introducing the attenuation factor $1/\ \| \boldsymbol{x} - \boldsymbol{x}_{\mathrm{cp}} \|^2$ (cf. [19]). Consequently, the approximation of $\boldsymbol{u}(\boldsymbol{x})$ now reads

$$\boldsymbol{u}(\boldsymbol{x}) = \frac{1}{\left\|\boldsymbol{x} - \boldsymbol{x}_{\mathrm{cp}}\right\|^2} \boldsymbol{A}\left(\boldsymbol{x} - \boldsymbol{x}_{\mathrm{cp}}\right)\ . \quad (11)$$

A critical point may be classified with respect to the eigenvalues of $\boldsymbol{A}$ (as proposed by Abraham and Shaw [1]): we distinguish attractors, repellors, saddle points, and rotation centers (see Fig. 1).

For our intended application, namely to interpret morphological changes of the brain, attractors and repellors describe areas of matter loss and growth, respectively, saddle points characterize configurations at barriers or membranes, and rotation centers may indicate local tissue shearing.

4 Estimation of Critical Points

When registering morphological changes we obtain vector fields – the displacements – that are not given on a continuous domain Ω, but on its discretization $\hat{\Omega}$ which reflects the finite resolution of the images. As discussed in the introduction, a critical point in our application domain is not infinitesimally small, but merely represents a zone where the vector field is attracted to or repelled from, for example.

In estimating critical points we rely on the contraction mapping theorem (e.g., [15]). From its mathematical foundation, our method is able to detect attractors or repellors, only. If a saddle point is unbalanced, i.e. the inflow of matter is not equal to the outflow, or if a rotation center attracts/repells during the morphological change that is registered, then we are able to detect them by contraction mapping.

4.1 Estimation algorithm

The algorithm to estimate attractors and repellers is subdivided in three steps: (1) cumulation and (2) clustering of attracting/repelling areas followed by (3) a phase portrait estimation to carry out a classification. In the following, with respect to an attractor the transforamtion $\boldsymbol{T} : \Omega \to \Omega$ will be applied, so that

$$\boldsymbol{T}(\boldsymbol{x}) = \boldsymbol{x} + \boldsymbol{u}(\boldsymbol{x})\,. \quad (12)$$

$\boldsymbol{T}$ is achieved by non-rigid registration (Sect. 2) and resides in an Euclidean reference frame. Accordingly, repellors can be attributed to

$$\boldsymbol{T}_{\mathrm{inv}}(\boldsymbol{x}) = \boldsymbol{x} - \boldsymbol{u}(\boldsymbol{x})\,. \quad (13)$$

4.1.1 Cumulation. To find a fix point $\boldsymbol{a}$ in the displacement field $\boldsymbol{u}$, we define a counter C on the dicretized domain $\hat{\Omega}$. Introducing a threshold t, and

$$\hat{\Omega}_{\mathrm{start}} := \left\{\boldsymbol{x} |\ \| \boldsymbol{u}(\boldsymbol{x}) \| > t,\ t > 0,\ \boldsymbol{x} \in \hat{\Omega}\right\}\ , \quad (14)$$

yields a set of starting points, that are linked to the attraction areas $\Theta(\boldsymbol{a}) \supset \{\boldsymbol{a}\}$ (i.e. an attraction area will contain more then just one point). Now consider the sequences

$\left[T^k(\boldsymbol{x})\right]_{k=0,1,\ldots}$. When reaching the condition $\boldsymbol{u}(T^k(\boldsymbol{x})) < t$ we increment the counter $C(T^k(\boldsymbol{x}))$. The distribution of the counter values $C(\boldsymbol{x})$ reflects the distribution of fix points of the vector field $\boldsymbol{u}$, after an iteration over all $\boldsymbol{x} \in \hat{\Omega}_{\text{start}}$.

4.1.2 Clustering. With two sequences $\left[T^k(\boldsymbol{x}_1)\right]_{k=0,1,\ldots}$ and $\left[T^l(\boldsymbol{x}_2)\right]_{l=0,1,\ldots}$ we will converge to the same fix point $\boldsymbol{a}$ if the following assumption is fulfilled

$$\boldsymbol{u}\left(T^k(\boldsymbol{x}_1)\right) < t \quad \wedge \quad \boldsymbol{u}\left(T^l(\boldsymbol{x}_2)\right) < t \rightarrow \left\| T^k(\boldsymbol{x}_1) - T^l(\boldsymbol{x}_2) \right\| < \alpha \tag{15}$$

for a certain value $\alpha > 0, \alpha \in \mathbb{R}$. The value of α should be chosen according to resolution of the grid $\hat{\Omega}$.

Attracting points are obtained by clustering the counter C. First, all locations $\boldsymbol{s} \in \hat{\Omega}$ where C has a local maximum are marked as point size cumulation areas Θ_s. Using a relative threshold $t(C(\boldsymbol{s}))$ the final size cumulation area is estimated: the area Θ_s establishes by adding neighboring grid points $\boldsymbol{x}$, as long as $C(\boldsymbol{x}) > t(C(\boldsymbol{s}))$. If during this search $C(\boldsymbol{x}) > C(\boldsymbol{s})$, then Θ_s is discarded as cumulation area since we found another maximum counter value in the vicinity of $\boldsymbol{s}$. After the area Θ_s has established its final size, its center of gravity is calculated, weighted with the counter values $C(\boldsymbol{x})$, $\boldsymbol{x} \in \Theta_s$ and then used as critical point location:

$$\boldsymbol{x}_{\text{cp}} := \frac{\sum_{\boldsymbol{x}\in\Theta_s} C(\boldsymbol{x})\boldsymbol{x}}{\sum_{\boldsymbol{x}\in\Theta_s} C(\boldsymbol{x})} \,. \tag{16}$$

4.1.3 Phase Portrait Estimation and Classification. Since we are seeking for an approximation of the vector field $\boldsymbol{u}(\boldsymbol{x})$ in the environment of a critical point $\boldsymbol{x}_{\text{cp}}$, we may substitute $\Delta\boldsymbol{x} := \boldsymbol{x} - \boldsymbol{x}_{\text{cp}}$ in (11) and yield:

$$\| \Delta\boldsymbol{x} \| \, \boldsymbol{u}\left(\boldsymbol{x}_{\text{cp}} + \Delta\boldsymbol{x}\right) = \boldsymbol{A}(\Delta\boldsymbol{x}) \,. \tag{17}$$

Accounting for a certain environment around $\boldsymbol{x}_{\text{cp}}$, with (17) we obtain an over-determined system of linear equations [19] which can be solved by using Householder transformations [21]. Since the phase portrait $\boldsymbol{A}$ is a 3×3 matrix, its eigenvalues can be calculated easily by solving the characteristic equation

$$\det(\boldsymbol{A} - \lambda\boldsymbol{I}) = 0$$

using Cardan's formula [4]. Critical points are classified by examining their eigenvalues (see Fig. 1).

5 Application – Visualization of shape change

We applied our algorithm to magnetic resonance (MR) images of a patient suffering from a neurodegenerative disease. A local destruction of brain tissue, which is removed during degeneration, is compensated by an increase in cerebro spinal fluid (CSF). Analyzing the pattern of matter loss is important to improve the understanding of the pathological process induced by the disease.

The patient was scanned twice within 12 month (Fig. 2). Both datasets were registered by the fluid dynamic, non-rigid approach described in Sect. 2. We obtained a displacement vector at every point of the reference image, corresponding to the shift of tissue during the time interval. Figure 3 serves as a first example to visualize such morphological change. The ventricular system (the low-intense cavities within the brain in Fig. 2) was segmented from the brain. The spatial pattern of shape change is visualized as follows: for each point on the ventricular surface, the displacement vector is decomposed into its normal and tangential components. Inward-pointing normals are coded in red, outward-pointing in blue; colour intensity reflects its magnitude. The scale is given in mm. The displacement vectors are shown as arrows. It is interesting to note that the ventricles are clearly enlarged, most notable in superior direction. This a consequence of a loss of brain tissue, resulting in an increase in the CSF volume. The superior orientation of the ventricular enlargement indicate a more profound tissue damage in the supra-ventricular compartment.

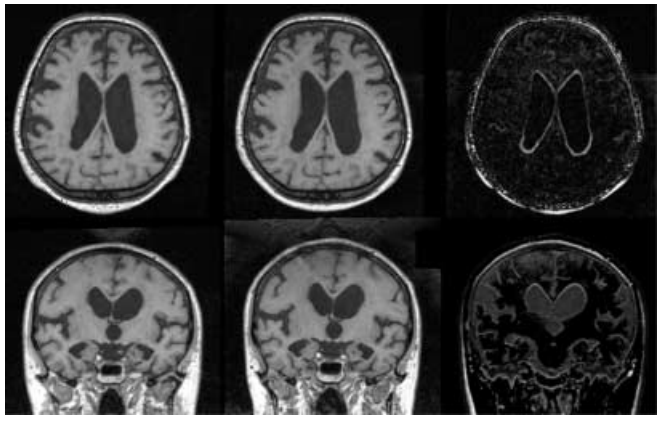

Fig. 2. Axial slice 90 (*top row*) and coronal slice 140 (*bottom row*) from $200 \times 256 \times 200$ voxel MR data sets taken 3 months (*left panel*) and 15 month (*middle panel*) after the patients' initial diagnostic findings. The *right panel* shows the difference between both images

From the displacement field we extracted about 110 critical points. To represent their properties, a colour scheme is implemented, where green and red indicate repelling or attracting property, and blue a rotation component. With this colour-code a critical point could be easily visualized: a repellor appears purely green, an attractor red, and a rotation center blue. Different types of saddle points may be distinguished by mixing the respective colours.

The set of critical points is dominated by a strong repellor locate in the pre-frontal CSF compartment (Fig. 4), and by several saddle points with strong repelling properties within the occipital CSF compartment (Fig. 5). A focus of matter loss is in the frontal lobes, leading to an increase of the CSF component close to the frontal pole. Displacement stream lines (Figs. 4 and 5) map the "flow" of tissue along the mid line structures (as a correlate of a global atrophy) and reveal a retraction of the brain in the frontal-occipital direction. The occipital saddle point (Fig. 5) can be interpreted as a backward shift of the brain, while pushing CSF in the repelling direction. As could be deduced by Fig. 4 the strongest deformations occur in the posterior portions of the first and second frontal gyrus on both hemispheres.

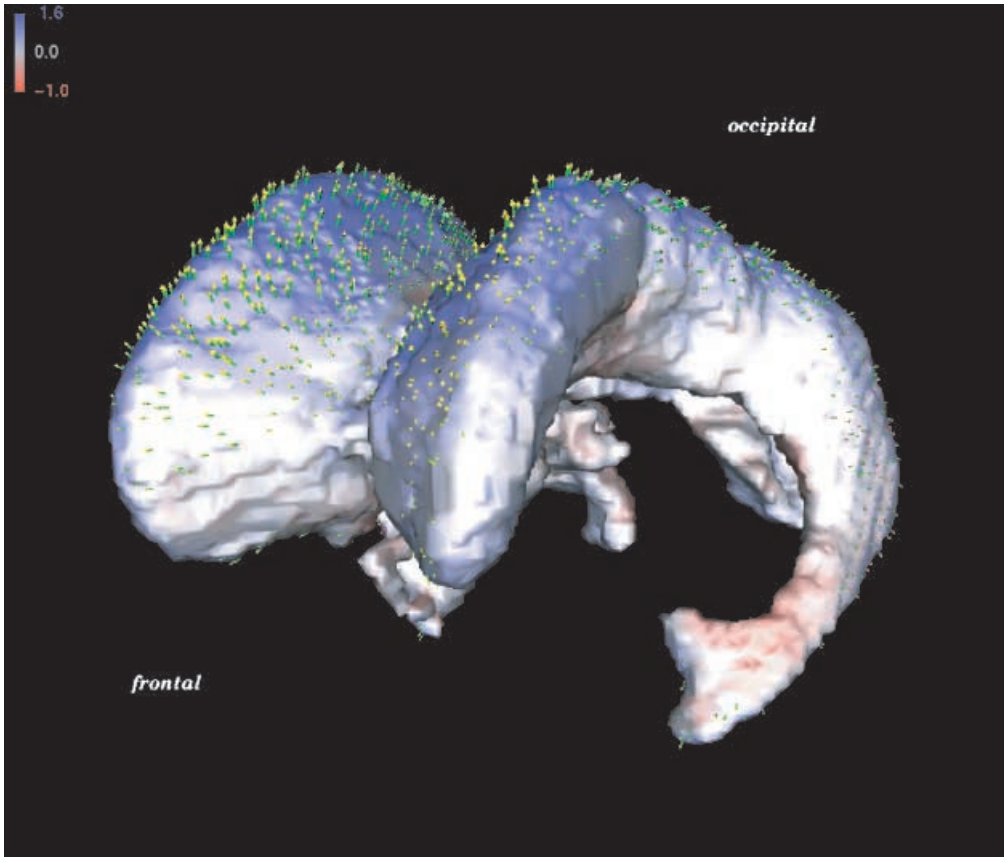

Fig. 3. Shape difference of a patients' ventricular system between two examination time points (see text). The *colour* indicate the orientation and magnitude of shape difference; *arrows* indicate the displacements. Note the overall enlargement of the system which is a consequence of the tissue loss (atrophy) of the surrounding brain

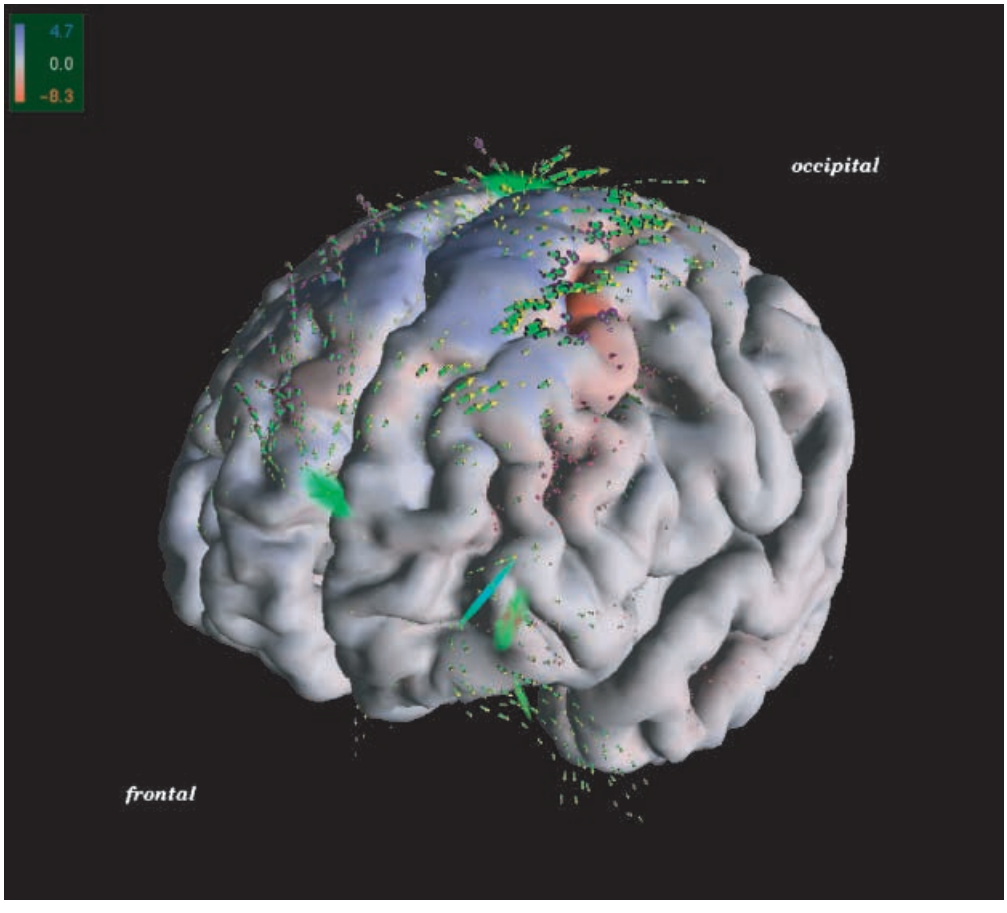

Fig. 4. Pattern of shape change of a patients' brain between two examination time points. Changes in morphology are visualized by colours; *red* and *blue* indicate inward and outward direction, respectively, and the magnitude of shape change perpendicular to the surface of the brain. The major displacement lines (*arrows*) depict the deformation lines. The critical point (repellor) within the frontal CSF compartment indicates a virtual flow in fronto-occipital direction

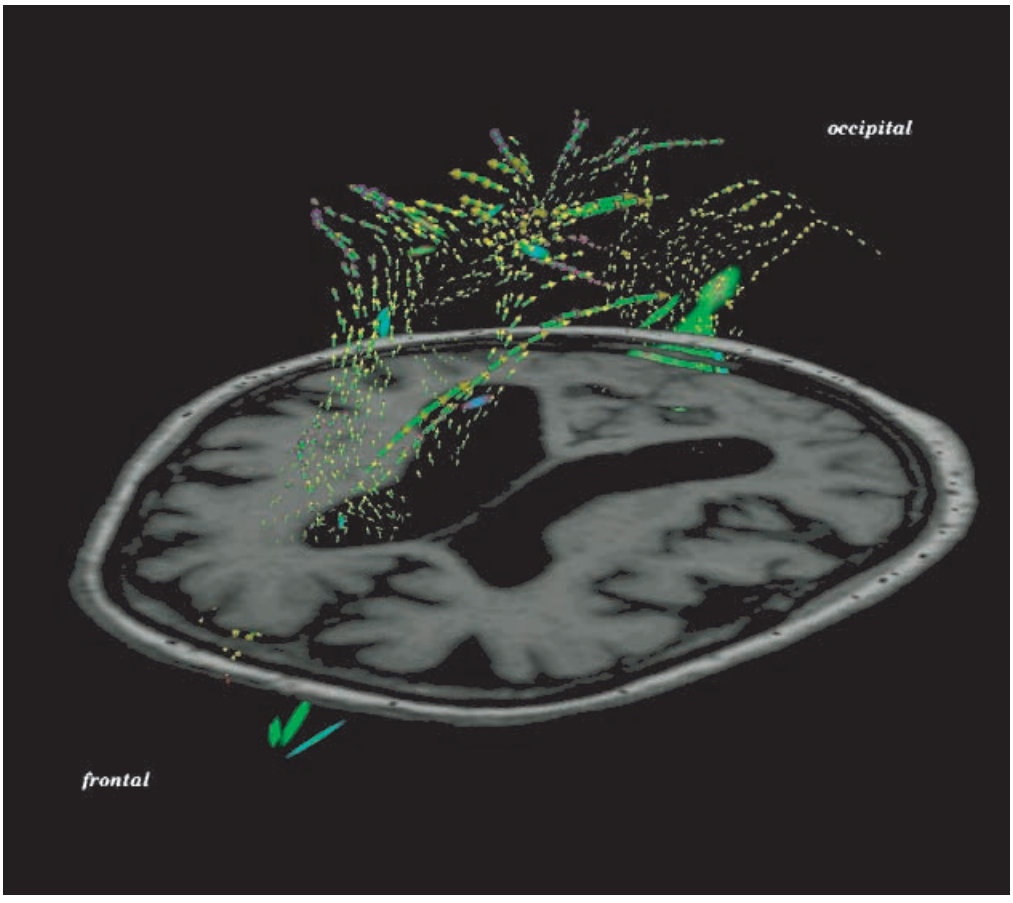

Fig. 5. View of an axial slice (taken from Fig. 4) with major displacements (*arrows*) and critical points of high magnitude. A repellor (green object) in the frontal cerebro-spinal fluid (CSF) and the displacement lines depict a virtual flow in occipital direction. Saddle points of type II (cf. Fig. 1) with strong repelling properties (*green part*) lie within the occipital CSF; those reveal a retraction of the brain. Small attractors (*red*) some with rotation properties (*red-magenta*) correspond to areas a regionally more profound matter loss

6 Conclusion

We proposed to describe displacement fields obtained from non-rigid registration of temporal series of MR images by its critical points. We introduced a novel method for finding critical points in discrete vector fields, which is based on contraction mapping.

However, our method fails to detect some specific critical points, namely rotation centers and balanced saddle points. Here, local measures based on the Jacobian [14] or global approaches like recently introduced by Polthier and Preuß [20] will be integrated with this method.

The advantage of conducting a biomedical analysis over simple visual comparison as carried out in clinical routine is obvious: the consequences of a neurodegenerative disease are understood as a circumscribed tissue loss leading to quantifiable deformations of the brain structures.

Acknowledgements. M.T. and G.W. are supported by the IST V programme of the European Union (SimBio project, No. 10378).

References

1. Abraham, R.H., Shaw, C.D.: Dynamics – The Theory of Behavior. 2nd edn. Redwood (Ca): Addison-Wesley 1992
2. Amit, Y.: A nonlinear variational problem for image matching. Soc. Ind. Math. 15(1), 207–224 (1994)
3. Bookstein, F.L.: Landmark methods for forms without landmarks: morphometrics of group differences in outline shape. Med. Image Anal. 1(3), 225–243 (1997)
4. Bronstein, I.N., Semendjajev, K.A., Musiol, G., Mühlig, H.: Taschenbuch der Mathematik (in german). 5th edn. Thun, Frankfurt/M.: Verlag Harry Deutsch 2001
5. Chistensen, G.E., Rabbit, R.D., Miller, M.I.: 3D brain mapping using deformable neuroanatomy. Phys. Med. Biol. 39, 609–618 (1994)
6. Christensen, G.E.: Deformable shape models for neuroanatomy. DSc.-thesis, Server Institue of Technology, Washington University, Saint Louis, 1994
7. Christensen, G.E., Johnson, H.J.: Consistent image registration. IEEE Trans. Medical Imag. 20(7), 568–582 (2001)
8. Christensen, G.E., Rabbitt, R.D., Miller, M.I.: Deformable templates using large deformation kinematics. IEEE Trans. Medical Imag. 5(10), 1435–1447 (Oct. 1996)
9. Gee, J.C., Reivich, M., Bajcsy, R.: Elastically deforming atlas to match anatomical brain images. J. Comp. Assisted Tomography 17, 255–236 (1993)
10. Gottlieb, D.H., Samaranayake, G.: The index of discontinuous vector fields. New York J. Math. 1, 130–148 (1995)
11. Grenander, U., Miller, M.I.: Computational anatomy: An emerging discipline. Quaterly Appl. Math. LVI(4), 617–694 (Dec. 1998)
12. Hege, H.-C., Polthier, K. (eds.): Mathematical visualization : algorithms, applications and numerics. Berlin, Heidelberg, New York: Springer 1998
13. Helman, J.L., Hesselink, L.: Representation and display of vector field topology in fluid flow data sets. IEEE Computer 22(8), 27–36 (August 1989)
14. Helman, J.L., Hesselink, L.: Visualizing vector field topology in fluid flows. IEEE Computer Graphics & Applications 11(3), 36–46 (May 1991)
15. Lu, N.: Fractal Imaging. San Diego, CA: Academic Press 1997
16. Maintz, J.B.A., Viergever, M.A.: A survey of medical image registration. Medical Image Analysis 2(1), 1–36 (1998)
17. Miller, M.I., Christensen, G.E., Amit, Y., Grenander, U.: Mathematical textbook of deformable neuroanatomies. In Proc. Natl. Acad. Sci. USA 90, pp. 11 944–11 948, 1993

18. Musse, O., Heintz, F., Armspach, J.-P.: Topology preserving deformable image matching using constraint hierachical parametric models. IEEE Trans. Medical Imag. 10(7), 1081–1093 (July 2001)
19. Philippou, P.A., Strickland, R.N.: Vector Field Analysis and Synthesis Using Three-Dimensional Phase Portraits. Graphical Models And Image Processing 6(59), 446–462 (1997)
20. Polthier, K., Preuß, E.: Detecting vector field singularities from potentials. http://www-sfb288.math.tu-berlin.de/~konrad/articles.html, 2001
21. Press, W.H., Teukolsky, S.A., Vetterling, W.T., Flannery, B.P.: Numerical Recipes in C. The Art of Scientific Computing. 2nd edn. New York: Cambridge Univ. Press 1992
22. Scheuermann, G., Hagen, H., Krüger, H.: Clifford algebra in vector field visualization. In: Hege, H.-C., Polthier, K. (eds.): Mathematical Visualization, pp. 343–351. Berlin, Heidelberg, New York: Springer 1998
23. Thévenaz, P., Ruttimann, U.E., Unser, M.: Iterative multi-scale registration without landmarks. In: Proc. ICIP-95, vol. III, pp. 228–231. Washington, DC., IEEE, 1995
24. Unser, M., Alroubi, A., Gerfen, C.R.: A multiresolution image registration procedure using spline pyramids. In: Mathematical Imaging: Wavelet Applications in Signal and Image Processing. Proc. SPIE, vol. 2034, pp. 160–170. San Diego, CA, 1993
25. Wollny, G.: MIA – a toolchain for Medical Image Analysis. http://mia.sourceforge.net, 2002
26. Wollny, G., Kruggel, F.: Computational cost of non-rigid registration algorithms based on fluid dynamics. accepted for IEEE Trans. Medical Imag., 2001